






Geophysical Research Letters®

RESEARCH LETTER

10.1029/2022GL102443

The Cross Equatorial Transport of the Hunga Tonga-Hunga Ha'apai Eruption Plume

M. R. Schoeberl¹ , Yi Wang¹ , R. Ueyama² , G. Taha³ , and W. Yu⁴ 

¹Science and Technology Corporation, Columbia, MD, USA, ²NASA Ames Research Center, Moffett Field, CA, USA,

³Morgan State University, Baltimore, MD, USA, ⁴Hampton University, Hampton, VA, USA

Key Points:

- Following the eruption, cross-equatorial transport of the water vapor occurs even though the meteorology does not appear to support this
- Infrared cooling associated with the enhanced water vapor after the eruption likely generated waves that produced the cross-equatorial flow
- Quasi-biennial oscillation-induced secondary circulation several months after the eruption also produced cross-equatorial transport of water vapor

Correspondence to:

M. R. Schoeberl,
mark.schoeberl@mac.com

Citation:

Schoeberl, M. R., Wang, Y., Ueyama, R., Taha, G., & Yu, W. (2023). The cross equatorial transport of the Hunga Tonga-Hunga Ha'apai eruption plume. *Geophysical Research Letters*, 50, e2022GL102443. <https://doi.org/10.1029/2022GL102443>

Received 6 DEC 2022

Accepted 25 JAN 2023

Author Contributions:

Conceptualization: M. R. Schoeberl

Data curation: M. R. Schoeberl, Yi Wang, W. Yu

Formal analysis: M. R. Schoeberl

Funding acquisition: R. Ueyama

Investigation: M. R. Schoeberl, R. Ueyama

Methodology: M. R. Schoeberl, G. Taha

Project Administration: M. R. Schoeberl, R. Ueyama

Resources: M. R. Schoeberl, G. Taha

Software: M. R. Schoeberl, Yi Wang

Supervision: M. R. Schoeberl, R. Ueyama

Validation: M. R. Schoeberl

Visualization: M. R. Schoeberl, Yi Wang

Writing – original draft: M. R. Schoeberl

Writing – review and editing: M. R. Schoeberl

© 2023. The Authors.

This is an open access article under the terms of the [Creative Commons Attribution License](https://creativecommons.org/licenses/by/4.0/), which permits use, distribution and reproduction in any medium, provided the original work is properly cited.

Abstract On 15 January 2022, the Hunga Tonga-Hunga Ha'apai (HT) eruption injected SO₂ and water into the middle stratosphere. Shortly after the eruption, the water vapor anomaly moved northward toward and across the equator. This northward movement appears to be due to equatorial Rossby waves forced by the excessive infrared water vapor cooling. Following the early eruption stage, persistent mid-stratospheric water vapor and aerosol layers were mostly confined to Southern Hemisphere tropics (Eq. to 30°S). However, during the spring of 2022, the westerly phase of the tropical quasi-biennial oscillation (QBO) descended through the tropics. The HT water vapor and aerosol anomalies were observed to again move across the equator coincident with the shift in the Brewer-Dobson circulation and the descent of the QBO shear zone.

Plain Language Summary The Hunga Tonga-Hunga Ha'apai (HT) submarine volcanic eruption on 15 January 2022, produced aerosol and water vapor plumes in the stratosphere. These plumes have persisted in the Southern Hemisphere. Following the eruption, we believe that the strong water vapor cooling forced equatorial Rossby waves whose circulation pushed the eruption plume into the Northern Hemisphere. Then, in April and May 2022, the descending quasi-biennial oscillation (QBO) transported more of the water vapor plume across the equator and widened the latitudinal extent of the aerosol plume. The spring 2022 change in the HT plume distribution shows the importance of forced Rossby waves and the QBO in stratospheric interhemispheric transport.

1. Introduction

The Hunga Tonga-Hunga Ha'apai (HT) (20.54°S, 175.38°W) erupted on 15 Jan. 2022, with a volcanic explosivity index of 5, comparable to Krakatoa eruption in 1883 (Carn et al., 2022). As shown in Microwave Limb Sounder (MLS) measurements (Millán et al., 2022, hereafter M22) and balloon sondes (Vomel et al., 2022) a significant amount of water vapor was injected into the southern hemisphere (SH) mid-stratosphere. HT also injected SO₂ which produced a distinctive aerosol layer that was detected by the Ozone Mapping and Profile Suite Limb Profiler (OMPS-LP) (Taha et al., 2022), although SO₂ injection was modest for an eruption of this size (Carn et al., 2022; M22). The MLS estimated water injection was up to 146 Tg (M22) or ~10% of the total stratospheric water vapor prior to the eruption. The water vapor and aerosol plumes from the HT eruption have persisted in the southern tropical mid-stratosphere for months, and the presence of water vapor led to a stratospheric cooling of ~4°K in March and April (Schoeberl et al., 2022, hereafter S22) due to the increased outgoing infrared (IR) radiation.

Trajectory simulations of the HT plume reported in S22 show that the plume should remain almost entirely in the SH, yet observations of both the aerosols and water vapor in the mid-stratosphere show the plume extending to 20°N. Below we show that there were two principal events where water vapor and aerosols were transported across the equator into the northern hemisphere (NH). The first event occurred within a month of the eruption. The second event was associated with descending quasi-biennial oscillation (QBO) shear zone. Below we analyze both events, starting with the QBO transport event. We will address these events in reverse order since the second event is more evident in the zonal mean observations.

2. Data Sets

As discussed in S22, we use MLS v5 for temperature and H₂O. The data quality for the HT anomaly is detailed in M22 and MLS data is described in Livesey et al. (2021). The MLS V5 algorithm quality flags and convergence

Writing – review & editing: M. R. Schoeberl, R. Ueyama, G. Taha, W. Yu

alerts were set for some plume profiles in the week or so after the eruption. However, even with the quality flag and convergence filters set, the data look reasonable and generally agree with sonde and other validation data. We restrict our constituent analysis to below 35 km. The MLS and OMPS data sets are averaged over 3 days and then averaged onto a $5^\circ \times 10^\circ$ latitude-longitude grid. For aerosols, we use OMPS-LP level-2 V2.1 997 nm extinction-to-molecular ratio data (aerosol extinction (AE)) from all three OMPS-LP slits (see Taha et al., 2021). Taha et al. (2022) indicated that the standard V2.1 released data (used in this study) provided the most accurate aerosol retrieval up to 36 km.

The Modern-Era Retrospective analysis for Research and Applications, Version 2 (MERRA2) reanalysis winds, temperatures, and heating rates used in this study are described in Gelaro et al. (2017). The residual circulation is computed using the formulas and notation in Andrews et al. (1987), specifically Equation 3.5.5b, $w^* = (\bar{Q} - \bar{\theta}_t) / \bar{\theta}_{oz}$ for computing the residual vertical velocity (w^*) from the zonal mean perturbation heating rate, \bar{Q} , where $\bar{\theta}$ is the zonal mean perturbation potential temperature. The $\bar{\theta}_t$ is computed from the change in daily $\bar{\theta}$ values. Our residual circulation vertical velocity agrees with vertical velocities derived from the analysis of the water vapor tape recorder (Schoeberl et al., 2008). The continuity equation is then used to compute the residual meridional velocity (v^*). MERRA2 data assimilation system does not include the water vapor measurements from MLS and thus does not account for the additional cooling from the water vapor anomaly which creates an anomalous circulation (Coy et al., 2022). To include that extra water vapor cooling we compute the total IR heating rate using 2022 MLS observed trace gases and temperatures using the radiative transfer model (RTM) described by Mlawer et al. (1997). We then we rerun the heating rate calculation assuming pre-eruption concentration of water vapor (~ 4 ppm). We compute the difference in radiative heating between the two computations and add that difference to the MERRA2 net heating rate, then recompute w^* . At 15°S , 26.8 km the MERRA2 residual circulation is upward with ~ 0.1 cm/s in January, decreasing to 0.03 cm/s in October. With the addition of the water vapor cooling the residual circulation is slower by 5% in January. The circulation is further reduced by $\sim 20\%$ by mid-February through March then the extra water vapor cooling effect fades through July. Over the equator the reduction in w^* is only a few percent over this period.

3. Analysis

In the next two sections we address the two cross equatorial constituent mixing events.

3.1. Cross Equatorial Transport Associated With the QBO

Unrelated to the HT eruption, during the 2022 spring and summer, the tropical stratospheric winds switched from easterly to westerly due to the QBO (see reviews by Hitchman et al., 2021; Baldwin et al., 2001). The descending westerly phase QBO produces a secondary circulation with downwelling at the equator—roughly the locus of the zero-wind line—and upwelling north and south of the equator (Plumb & Bell, 1982). This secondary circulation will alter the distribution of trace gases such as ozone, N_2O , water vapor, and other long lived trace gases (Hitchman et al., 2021; Trepte & Hitchman, 1992). The induced circulation contributes to the mixing of the lower stratospheric trace gases within the tropics, and between the hemispheres as is evident in observational data sets (Anstey et al., 2022; Baldwin et al., 2001; Randel et al., 1998). The simple models of the QBO assume that the secondary circulation is symmetric about the equator so cross equatorial transport would not be possible in that framework. Indeed, the symmetric circulation produces a cross-equatorial transport barrier as first noted by Trepte and Hitchman (1992). The observed structure of the QBO and Brewer-Dobson (BD) upwelling circulation is not perfectly symmetric and the cross-equatorial circulation can be quite strong (Randel et al., 1993, 1999). The QBO circulation can also exhibit asymmetry due to hemispheric differences in the upward gravity wave momentum flux and extra-tropical wave breaking (Anstey et al., 2022; Baldwin et al., 2001; Hitchman et al., 2021; Kinnersley, 1999; Peña-Ortiz et al., 2008).

Figures 1a–1f show the evolution of the 3-day average OMPS-LP AE (Taha et al., 2021) and MLS zonal mean water vapor. The MERRA2 zonal mean zero wind line is also shown along with the residual circulation streamlines. The observations are shown at the first of each month except for August where we show the 12th, because OMPS-LP was offline at beginning of the month. We begin in March when the HT water vapor field becomes zonally well mixed as indicated by the MLS observations (Figure 2a). The initial water vapor and aerosol

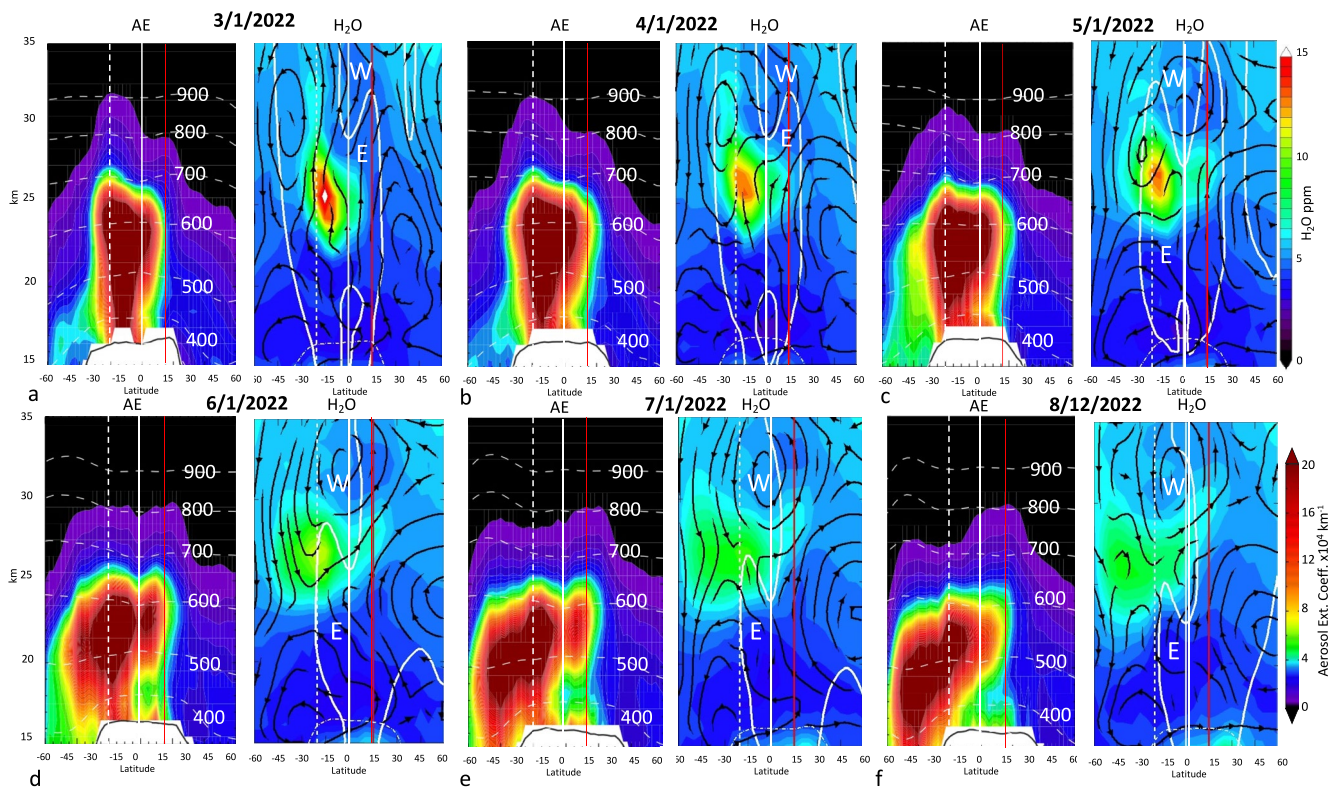


Figure 1. Sequence of zonal mean 997 nm aerosol extinction (AE) and water vapor plots starting March 1 (a), April 1 (b), etc. dates in month/day/year format are above the figures. Because Ozone Mapping and Profile Suite Limb Profiler was not operational on August 1, we plot August 12 in part (f). The plots are the individual days; the data is averaged over 3 adjacent days. The residual circulation streamlines (black) and zero zonal wind line (white) is shown overlaid on the H₂O plots. The “W” and “E” indicate westerly and easterly regimes. Vertical white and red lines indicate 0° and 15°N for reference; dashed line is the latitude of HT. Potential temperature surfaces are indicated on the AE plots (K).

distribution is primarily south of 10°N. The figure shows that the water vapor is concentrated mostly above 20 km where the warmer stratosphere can support higher concentrations (S22). The aerosols are initially distributed from the tropopause to approximately the same altitude as the water vapor, but the two distributions slowly separate in time with the water vapor anomaly rising while the peak altitude of the aerosol anomaly descends (S22).

Figure 1 sequence shows the descent of the tropical QBO westerlies. Between March 1 and April 1 there is little descent of the westerlies above about 30 km. Then, beginning in April, the westerlies begin to descend rapidly. By May 1, the top of the aerosol distribution has spread deeper into the SH and a secondary maximum in water vapor has appeared in the NH (see arrow). The residual streamlines shown overlaid on the water vapor plots provide an explanation for the changing aerosol and water vapor distributions. In March, the ~20°S upward transport of water vapor is consistent with the residual circulation. In April, the streamlines shift, and the residual circulation begins to transport water vapor toward the north. By May 1 (Figure 1c), a lobe of water vapor has formed in the NH moving north of 15°N. The northward residual circulation is still present on May 1 but has weakened, although the water vapor anomaly continues to slowly expand northward. Also by May 1, at 22 km a lobe of aerosols develops north of the equator, and the residual circulation transports the aerosol distribution further south.

By July, above the tropical zero-wind line within the westerly wind regime, the ascending branch of the residual circulation in the NH tropics reinforces a descending branch in the SH tropics. This circulation cell transports dry air downward into the HT anomaly while pulling the northern edge of the anomaly upward. The transport creates the U-shaped structure in water vapor seen in July and August. The aerosol anomaly retreats southward. The residual circulation at the lower altitudes is southward explaining this retreat.

The upward propagating tropical waves that produce QBO deposit their momentum in the shear zone centered on the zero-wind line. As wave momentum is deposited in the shear zone, the zonal wind speed changes, moving the shear zone downward. Observations and models show that the secondary circulation surrounding the QBO

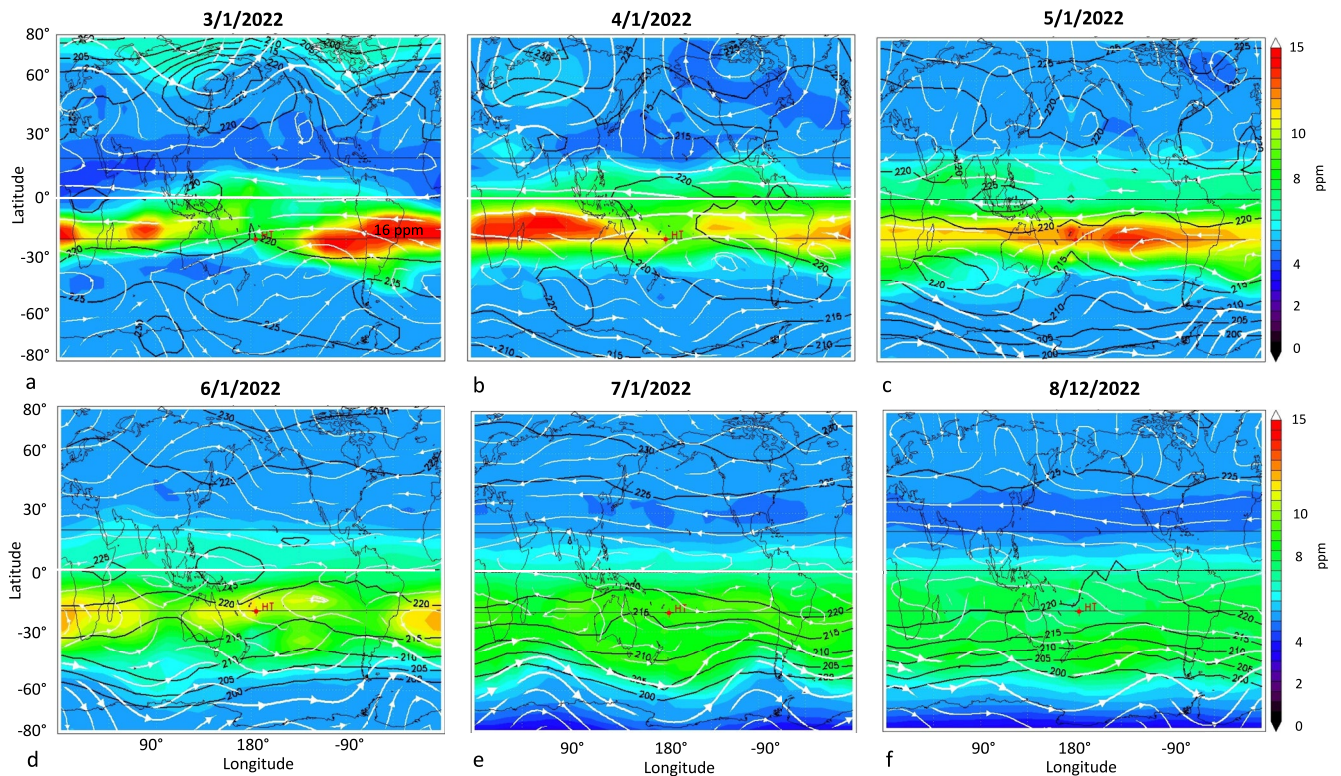


Figure 2. Maps of the Microwave Limb Sounder (MLS) water vapor at 26.8 km (~21.5 hPa) using 3 days of data centered on the date shown as in Figure 1. Temperatures (also from MLS) are shown with black contours. The streamlines (white arrows) are generated using Modern-Era Retrospective analysis for Research and Applications, Version 2 winds. The dates correspond to those in Figure 1.

momentum deposition region extends ~5 km below the shear zone (Baldwin et al., 2001; Hitchman et al., 2021) and QBO wind anomalies extend horizontally to ~15° on either side of the equator (Dunkerton & Delisi, 1985).

We can interpret the changes in water vapor in terms of the QBO induced transport circulation as follows: Between March 1 and April 1, the QBO descent is very slow, which means that there is little wave momentum being deposited at upper levels. The QBO secondary circulation is weak, and the stratospheric circulation is dominated by the seasonal BD circulation. The 24–26 km HT water vapor anomaly is confined mostly to the SH at this stage. Starting in April, the westerlies begin to descend, the meridional residual circulation below the zero-wind line begins to transport water vapor northward across the equator. Note that the residual circulation in the tropics, which is a combination of seasonal BD and QBO circulations, is not symmetric across the equator and the northward transport cell extends across the equator (Randel et al., 1999). In 2022, this asymmetry may have been amplified by additional water vapor cooling in the SH (S22). As the zero-wind line continues to descend into the HT plume, the residual circulation weakens, and transport slows (June, July, ~26 km). This weakening can be partly attributed to a seasonal change in the BD circulation which is strongest during boreal winter (Plumb, 2002). Thus, the observed changes in the HT water vapor distribution are broadly consistent with the transport circulation surrounding the descending QBO (Baldwin et al., 2001; Hitchman et al., 2021; Peña-Ortiz et al., 2008) combined with the seasonally changing BD circulation (Gray & Dunkerton, 1990; Randel et al., 1999).

From the simple models of the QBO, we expect that waves to amplify as the shear zone approaches from above, and then wave amplitudes should decrease as the shear zone passes. The change in wave activity occurs due to conservation of wave action density—the wave energy divided by the frequency (Andrews et al., 1987, Equation 4A.12). As the wave propagates upward toward its critical line, the group velocity decreases, and the wave amplitude increases. This should enhance the variance in trace gas fields if a tracer gradient is present. Figure 2 shows maps of the MLS water vapor distribution and temperatures at 26.8 km (~21.5 hPa) along with streamlines from MERRA2 winds. The H₂O distribution on April 1 shows a zonal wave-2 structure at the northern edge of the anomaly along with the temperature and wind streamlines. The tropical wave structure does not match the wave-1

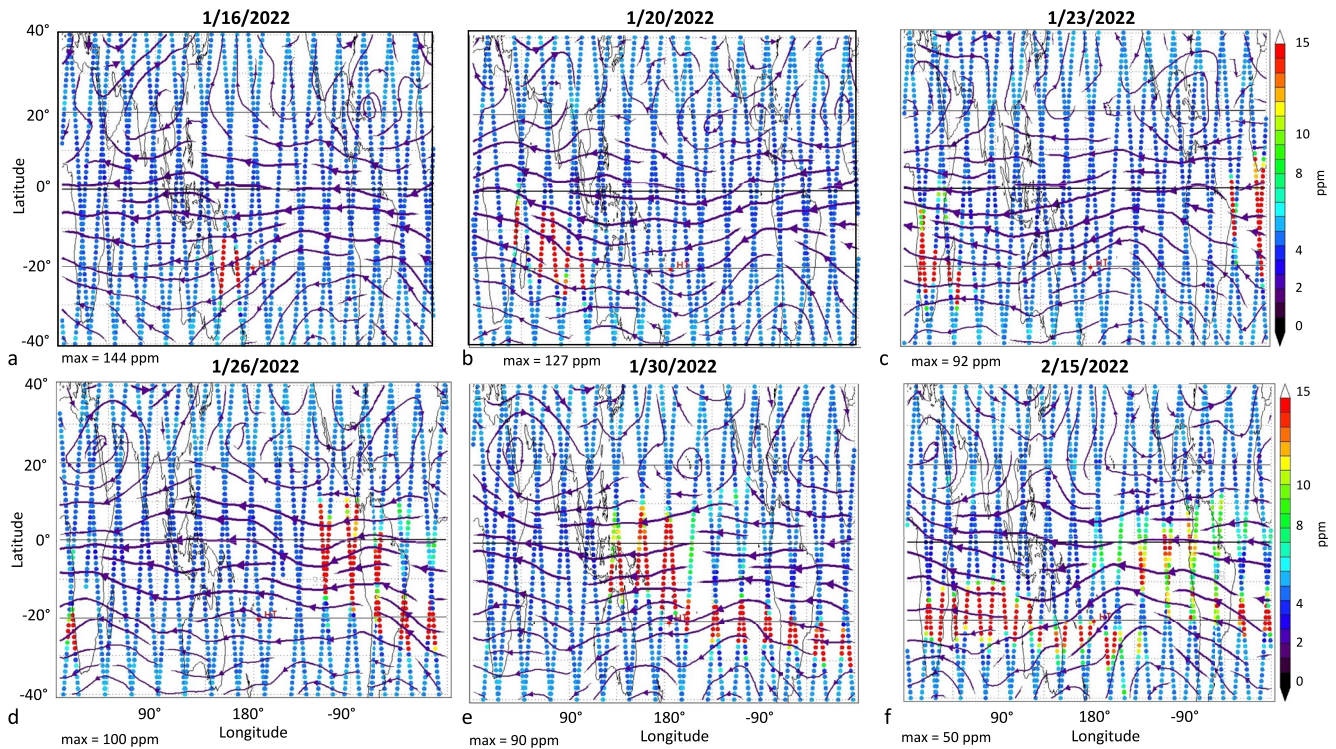


Figure 3. Maps of Microwave Limb Sounder observed water vapor anomaly at 26.8 km following the HT eruption.

Dates are shown at the top of each figure for parts a–f. The peak water vapor mixing ratio is indicated at the lower left of each figure. Streamlines from Modern-Era Retrospective analysis for Research and Applications, Version 2 are shown as arrows.

seen at higher latitudes so this wave is likely not propagating into the tropics from higher latitudes. By May 1 the water vapor distribution uniformly extends to 20°N and the wave structures in tropical wind and temperature fields have decreased. The wave structure seen on April 1 might be expected from the amplification of the Kelvin wave as it approaches the critical line. Then, in the subsequent months (June–August), the water vapor distribution becomes more zonally uniform along with the wind and temperature fields. We have examined the time variation of the water vapor variance (not shown) at 26.8 km and indeed it increases as the QBO moves downward to this altitude and then abruptly decreases with the passage of the shear zone. The equatorial seasonal upward residual circulation also switches from ascending to descending as the QBO shear zone passes then returns to ascending as expected from the simple QBO models (Plumb & Bell, 1982).

3.2. Cross Equatorial Transport Shortly After the Eruption

Figure 3 shows maps of water vapor and streamlines at 26.8 km for selected days following the eruption. Rather than average the data over 3 days, we show the location of MLS profiles and the water vapor mixing ratio. The maximum water vapor is shown at the lower left of each figure. Figure 3a shows the distribution on January 16. As noted by Millán et al. (2022), MLS scans do not completely catch the locally concentrated plume. Figure 3b (January 20) shows the anomaly moving toward the equator roughly following the streamlines. By January 23 the anomaly has crossed the equator and reached 10°N even though streamlines are mostly zonal. The MERRA2 meridional flow at this altitude is <2 m/s at ±15°N which means that it would take ~10 days for the plume to transit from 5°S to 10°N, but this transit took place in about 3–4 days. On January 26 the anomaly has reached 10°N. Because of the strong meridional wind shear, and faster winds at the equator, move the equatorial portion of the anomaly ahead of the slower moving more poleward component (Figures 3d–3f). Examination of levels below 26.8 km shows that the anomaly is ~3 km deep and is moving uniformly.

Why did the HT water vapor anomaly move more rapidly to the north between January 20 and January 23? One possible explanation for the movement of the plume toward the equator is that the IR cooling from the water vapor anomaly excited a Rossby wave that advected the water vapor anomaly toward the equator. The simple

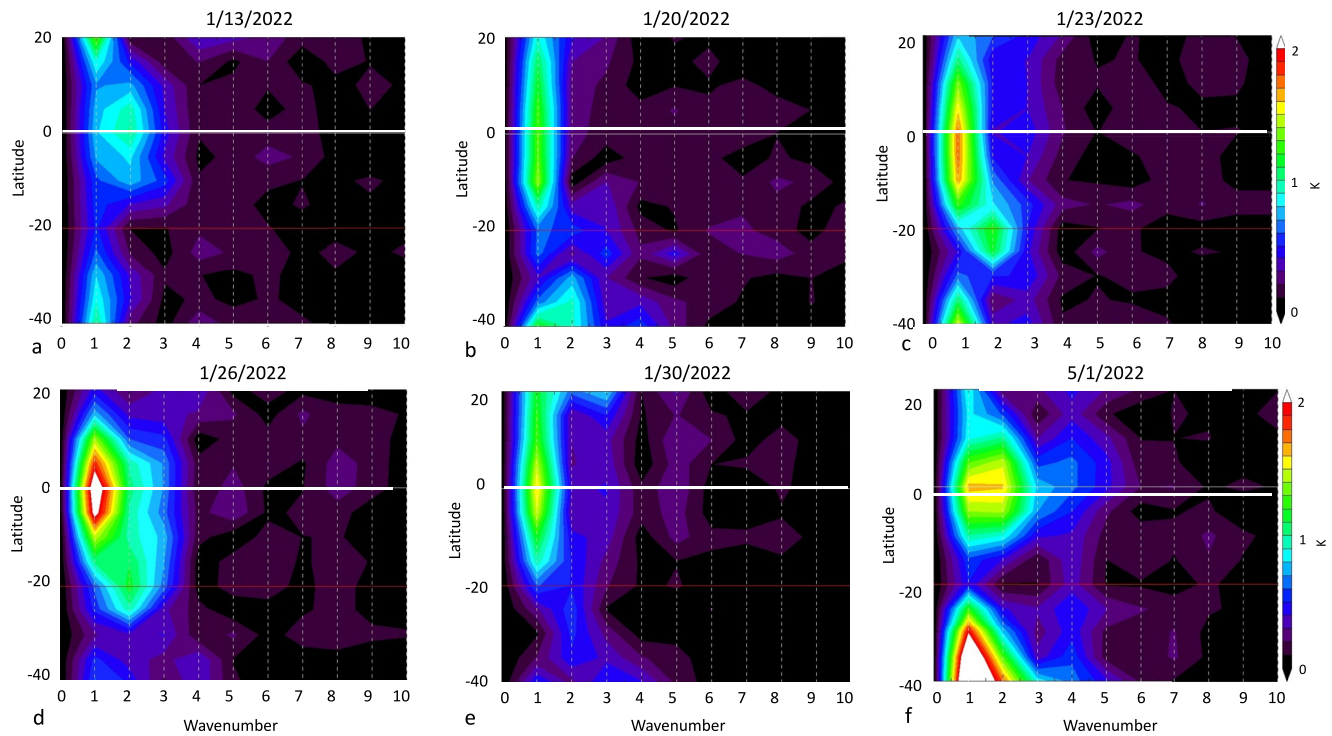


Figure 4. Microwave Limb Sounder temperature wave amplitudes at 26.8 km versus latitude. Zonal mean temperature is removed. Dates are indicated above each plot for parts a–f. Red line indicates the latitude of HT, white line is the equator. Parts (b–e) correspond to panels (b–e). Wave 0, the zonal mean, is removed.

circulation models of thermally forced equatorial Rossby waves provided by Gill (1980, Figure 3) would apply. In this scenario, the IR cooling by the water vapor anomaly creates a local pressure anomaly which excites a Rossby wave, creates cross equatorial flow, which advects part of the anomaly across the equator. Because this cooling is not included in the MERRA2 reanalysis (because the MLS water vapor is not assimilated), the strength of the MERRA2 meridional wind is probably underestimated. We have computed the additional IR cooling for January 19, using the RTM, and at 27.5 km it is ~ 3 K/day reaching ~ 5 K/day at 30 km. Our estimate of the radiative forcing agrees with Silletto et al. (2022) who also noted that the aerosol plume has almost no net radiative impact. This magnitude of localized cooling just off the equator is sufficient to force the Rossby wave (Gill, 1980). After the plume is advected toward the equator and the water vapor distribution becomes more zonal, the non-zonal cooling rate would decrease and the Rossby wave amplitude would decrease as well.

A zonal spectral analysis of the temperature fields provides more insight. Figure 4 shows a zonal wavenumber spectrum at 26.8 km using 3-day average MLS perturbation temperatures. Figure 4a shows the pre-eruption wave amplitudes versus latitude on January 13, indicating that the ambient waves are weak, with a ~ 1 K amplitude Kelvin wave centered on the equator. On January 20 (Figures 4b and 3b), just following the eruption, conditions are immediately different. The thermal amplitude of wave one has nearly doubled north of the HT eruption latitude. Spectral analysis shows that zonal wave one moves west at about 24° longitude/day (~ 31 m/s) during late January. The average equatorial flow speed on January 26 at this altitude is westward at 31.4 m/s. Thus, the wave is nearly stationary with respect to the flow. The thermal disturbance associated with the spatially narrow plume spreads energy into the higher wavenumbers at 20° S. By January 26, (Figures 4c and 3c) wave one has increased to 1.5 K at about 5° S and 2.4 K at the equator. A wave two disturbance has also formed at the HT latitude. The waves subsequently begin to decrease in amplitude as seen on January 30 (Figures 4e and 3e). Wave amplitudes continue to decrease during February (not shown) to pre-eruption amplitudes.

The thermal wavenumber analysis is consistent with the idea that H_2O IR cooling generates equatorial Rossby waves shortly after the eruption. The fact that the phase speed of the Rossby wave is nearly identical to the flow carrying the water vapor anomaly is consistent with Gill forced waves. We can make a rough estimate of the enhanced meridional circulation (v') generated by the wave using the thermal wind equation and assuming that

the heating anomaly has the vertical scale of a scale height (~ 7 km). v' is given by $v' = mRT'/f$, where f is the Coriolis frequency at 15°S , R is the dry air gas constant, m is the zonal wavenumber and T' is the temperature. Using $T' = 2$ K, $v' \sim 2.5$ m/s. Adding this to the background meridional flow of 2 m/s, the transit time to move the water vapor from 5°S to 15°N is 4.5 days. This is much closer to the observed anomaly transit time from January 20–23 period. Finally, to connect with the QBO discussion in Section 3.1, Figure 4f shows the wave amplitudes on April 1. The figure clearly shows wave amplification as the QBO shear line approaches 26 km when compared to Figure 4a.

4. Summary and Discussion

The HT injection of aerosols and water into the mid-stratosphere provides an unprecedented opportunity to examine our understanding of tropical stratospheric dynamics and interhemispheric transport of trace gases. Trajectory simulations of the plume spread show almost no mid-stratospheric transport across the equator during first 5 months after the eruption (S22); nonetheless, at least two cross equatorial transport events occurred. The first, shortly after the eruption and the second during April and May 2022. Explanation for these events is given in this paper.

The initial HT plume moved $\sim 30^\circ$ northward within the first few weeks after the eruption (Figure 3) even though the pre-eruption flow was approximately zonal with weak wave activity at tropical latitudes. The northward advection of the plume may have resulted from strong H_2O IR cooling of the plume, and the subsequent non-zonal radiative cooling would force an equatorial Rossby wave response (Gill, 1980). The resulting cross equatorial flow would have transported the plume meridionally. Wavenumber analyses of MLS temperatures show a coincidental rapid increase in wave one and two across throughout tropics, consistent with this hypothesis. These anomalies move with the flow as expected with forced waves. The meridional cross-equatorial velocity may have more than doubled due to the presence of these waves. By the end of January, the forced Rossby waves are subsiding as the water vapor plume shears out and the localized (non-zonal) forcing decreases.

During March, the QBO shear zone began to descend through the tropics switching the zonal winds from easterlies to westerlies in the mid-stratosphere. The induced circulation produced by wave momentum deposition combined with the BD circulation produces a second cross-equatorial transport event. This event is most evident at ~ 26 km where the meridional water vapor gradient is large. The QBO transport is clearly observed in the MLS water vapor mixing ratios, and, as diagnosed through the residual circulation, is consistent with earlier analyses of QBO dynamics (Baldwin et al., 2001; Randel et al., 1999). The circulation well below the QBO shear zone appears to prevent a similar spread in the lower altitude aerosol distribution.

The fact that these two transport events were not reproduced by trajectory simulations (S22) suggests the need for additional improvements in MERRA2 tropical dynamics, and the need for stratospheric water vapor assimilation—at least during the HT period. Finally, although the SH and NH tropical stratospheres appear to be relatively isolated under normal conditions (Hitchman et al., 2021), the evolution of the HT plume reveals that the QBO can play an important, albeit episodic, role in trace gas exchange between the two hemispheres.

Data Availability Statement

MERRA-2 Reanalysis data—Gelaro et al. (2017). MERRA-2 data are obtained from the Global Modeling and Assimilation Office (GMAO), *inst3_3d_asm_Cp: MERRA-2 3D IAU State, Meteorology Instantaneous 3-hourly (p-coord, 0.625x0.5L42), version 5.12.4* at <https://doi.org/10.5067/WWQSQ8IVFW8>. The data are public with unrestricted access (registration required). The RTM used to estimate H_2O cooling rates is from Atmospheric and Environmental Research and can be freely downloaded at http://rtweb.aer.com/rtrtm_frame.html. OMPS-LP data, Taha et al. (2021), is available at https://disc.gsfc.nasa.gov/datasets/OMPS_NPP_LP_L2_AER_DAILY_2/summary, DOI: [10.5067/CX2B9NW6FI27](https://doi.org/10.5067/CX2B9NW6FI27). The algorithm is documented in Taha et al. (2021). Data are public with unrestricted access (registration required). Aura MLS Level 2 data, Livesey et al. (2021) JPL D-33509 Rev. C, is available at <https://disc.gsfc.nasa.gov/datasets?page=1&keywords=AURA%20MLS>. The temperature data is available at https://acdisc.gesdisc.eosdis.nasa.gov/data/Aura_MLS_Level2/ML2T.004/. The V4 water vapor data is available at https://acdisc.gesdisc.eosdis.nasa.gov/data/Aura_MLS_Level2/ML2H2O.004/. The V5 water vapor data is available at https://acdisc.gesdisc.eosdis.nasa.gov/data/Aura_MLS_Level2/ML2H2O.005/.

Acknowledgments

This work was supported under NASA Grants NNX14AF15G, 80NSSC21K1965, and 80NSSC20K1235.

References

Andrews, D. G., Holton, J. R., & Leovy, C. B. (1987). *Middle atmosphere dynamics* (Vol. 489). Academic Press. ISBN: 9780120585762.

Anstey, J. A., Osprey, S. M., Alexander, J., Baldwin, M. P., Butchart, N., Gray, L., et al. (2022). Impacts, processes, and projections of the quasi-biennial oscillation. *Nature Reviews Earth & Environment*, 3(9), 588–603. <https://doi.org/10.1038/s43017-022-00323-7>

Baldwin, M. P., Gray, L. J., Dunkerton, T. J., Hamilton, K., Haynes, P. H., Randel, W. J., et al. (2001). The quasi-biennial oscillation. *Review of Geophysics*, 39(2), 179–229. <https://doi.org/10.1029/1999RG000073>

Carn, S. A., Krotkov, N. A., Fisher, B. L., & Li, C. (2022). Out of the blue: Volcanic SO₂ emissions during the 2021–2022 Hunga Tonga–Hunga Ha’apai eruptions. *Frontiers Earth Science*, 13. <https://doi.org/10.3389/feart.2022.976962>

Coy, L., Newman, P., Wargan, K., Partyka, G., Strahan, S., & Pawson, S. (2022). Stratospheric circulation changes associated with the Hunga Tonga–Hunga Ha’apai eruption. *Geophysical Research Letters*, 49(22), e2022GL100982. <https://doi.org/10.1002/essoar.10512388.1>

Dunkerton, T. J., & Delisi, D. P. (1985). Climatology of the equatorial lower stratosphere. *Journal of the Atmospheric Sciences*, 42(4), 376–396. [https://doi.org/10.1175/1520-0469\(1985\)042<0376:cotels>2.0.co;2](https://doi.org/10.1175/1520-0469(1985)042<0376:cotels>2.0.co;2)

Gelaro, R., McCarty, W., Suarez, M. J., Todling, R., Molod, A., Takacs, L., et al. (2017). The modern-era retrospective analysis for research and applications, version 2 [Dataset]. *Journal of Climate*, 30(14), 5419–5454. <https://doi.org/10.1175/jcli-d-16-0758.1>

Gill, A. E. (1980). Some simple solutions for heat-induced tropical circulation. *Quarterly Journal of the Royal Meteorological Society*, 106(449), 447–462. <https://doi.org/10.1002/qj.49710644905>

Gray, L. J., & Dunkerton, T. J. (1990). The role of the seasonal cycle in the quasi-biennial oscillation of ozone. *Journal of the Atmospheric Sciences*, 47(20), 2429–2451. [https://doi.org/10.1175/1520-0469\(1990\)047<2429:trotsc>2.0.co;2](https://doi.org/10.1175/1520-0469(1990)047<2429:trotsc>2.0.co;2)

Hitchman, M., Yoden, S., Haynes, P. H., Kumar, V., & Tegtmeier, S. (2021). An observational history of the direct influence of the stratospheric quasi-biennial oscillation on the tropical and subtropical upper troposphere and lower stratosphere. *Journal of the Meteorological Society of Japan*, 99(2), 239–267. <https://doi.org/10.2151/jmsj.2021-012>

Kinnersley, J. S. (1999). Seasonal asymmetry of the low- and middle-latitude QBO circulation anomaly. *Journal of the Atmospheric Sciences*, 56(9), 1140–1153. [https://doi.org/10.1175/1520-0469\(1999\)056<1140:saotla>2.0.co;2](https://doi.org/10.1175/1520-0469(1999)056<1140:saotla>2.0.co;2)

Livesey, N., Read, W. G., Wagner, P. A., Froidevaux, L., Santee, M. L., Schwartz, M. J., et al. (2021). Earth observing system (EOS) Aura Microwave limb sounder (MLS) version 5.0x level 2 and 3 data quality and description document. JPL D-105336 Rev A Retrieved from https://mls.jpl.nasa.gov/data/v5-0_data_quality_document.pdf

Millán, L., Santee, M. L., Lambert, A., Livesey, N. J., Werner, F., Schwartz, M. J., et al. (2022). The Hunga Tonga–Hunga Ha’apai hydration of the stratosphere. *Geophysical Research Letters*, 49, e2002GL099381. <https://doi.org/10.1029/2022GL099381>

Mlawer, E. J., Taubman, S. J., Brown, P. D., Iacono, M. J., & Clough, S. A. (1997). RRTM, a validated correlated-k model for the longwave. *Journal of Geophysical Research*, 102(D14), 16663–16682. <https://doi.org/10.1029/97jd00237>

Peña-Ortiz, C., Ribera, P., Garcí’a-Herrera, R., Giorgetta, M. A., & Garcí’a, R. R. (2008). Forcing mechanism of the seasonally asymmetric quasi-biennial oscillation secondary circulation in ERA-40 and MAECHAM5. *Journal of Geophysical Research*, 113(D16), D16103. <https://doi.org/10.1029/2007JD009288>

Plumb, R. A. (2002). Stratospheric transport. *Journal of the Meteorological Society of Japan*, 80(4B), 793–809. <https://doi.org/10.2151/jmsj.80.793>

Plumb, R. A., & Bell, R. C. (1982). A model of the quasi-biennial oscillation on an equatorial beta-plane. *Quarterly Journal of the Royal Meteorological Society*, 108(456), 335–352. <https://doi.org/10.1002/qj.49710845604>

Randel, W. J., Gille, J., Roce, A., Kumer, J., Mergenthaler, J., Waters, J., et al. (1993). Stratospheric transport from the tropics to middle latitudes by planetary-wave mixing. *Nature*, 365(6446), 533–535. <https://doi.org/10.1038/365533a0>

Randel, W. J., Wu, F., Russel, J. M., III, Roche, A., & Waters, J. (1998). Seasonal cycles and QBO variations in stratospheric CH₄ and H₂O observed in UARS HALOE data. *Journal of the Atmospheric Sciences*, 55(2), 163–185. [https://doi.org/10.1175/1520-0469\(1999\)056<0457:GQCDFU>2.0.CO;2](https://doi.org/10.1175/1520-0469(1999)056<0457:GQCDFU>2.0.CO;2)

Randel, W. J., Wu, F., Swinbank, R., Nash, J., & O’Neill, A. (1999). Global QBO circulation derived from UKMO stratospheric analyses. *Journal of the atmospheric sciences*, 56(4), 457–474. [https://doi.org/10.1175/1520-0469\(1998\)055<0163:SCAQVI>2.0.CO;2](https://doi.org/10.1175/1520-0469(1998)055<0163:SCAQVI>2.0.CO;2)

Schoeberl, M. R., Douglass, A. R., Stolarski, R. S., Pawson, S., Strahan, S. E., & Read, W. (2008). Comparison of lower stratospheric tropical mean vertical velocities. *Journal of Geophysical Research*, 113(D24), D24109. <https://doi.org/10.1029/2008JD010221>

Schoeberl, M. R., Wang, Y., Ueyama, R., Taha, G., Jensen, E., & Yu, W. (2022). Analysis and impact of the Hunga Tonga–Hunga Ha’apai stratospheric water vapor plume. *Geophysical Research Letters*, 49(20), e2022GL100248. <https://doi.org/10.1029/2022GL100248>

Sillette, P., Podglagen, A., Belhadji, R., Boichu, M., Carboni, E., Cuesta, J., et al. (2022). The unexpected radiative impact of the Hunga Tonga eruption of January 15, 2022. *Communications Earth & Environment*, 3(1), 288. <https://doi.org/10.1038/s43247-022-00618-z>

Taha, G., Loughman, R., Colarco, P., Zhu, T., Thomason, L., & Jaross, G. (2022). Tracking the 2022 Hunga Tonga–Hunga Ha’apai aerosol cloud in the upper and middle stratosphere using space-based observations. *Geophysical Research Letters*, 49(19), e2022GL100091. <https://doi.org/10.1029/2022GL100091>

Taha, G., Loughman, R., Zhu, T., Thomason, L., Kar, J., Rieger, L., & Bourassa, A. (2021). OMPS LP Version 2.0 multi-wavelength aerosol extinction coefficient retrieval algorithm. *Atmospheric Measurement Techniques*, 14(2), 1015–1036. <https://doi.org/10.5194/amt-14-1015-2021>

Trepte, C. R., & Hitchman, M. H. (1992). Tropical stratospheric circulation deduced from satellite aerosol data. *Nature*, 355(6361), 626–628. <https://doi.org/10.1038/355626a0>

Vömel, H., Evan, S., & Tully, M. (2022). Water vapor injection into the stratosphere by Hunga Tonga–Hunga Ha’apai. *Science*, 377(6613), 1444–1447. <https://doi.org/10.1126/science.abq2299>